Complete mapping of energy transfer pathways in the plant light-harvesting complex Lhca4

Tros, Martijn; Novoderezhkin, Vladimir I; Croce, Roberta; van Grondelle, Rienk; Romero, Elisabet

Link to publication in VU Research Portal

Check for updates

Complete mapping of energy transfer pathways in the plant light-harvesting complex Lhca4†

Martijn Tros, [iD] *[a] Vladimir I. Novoderezhkin,[b] Roberta Croce, [iD] [a]
Rienk van Grondelle[a] and Elisabet Romero[c]

The Lhca4 antenna complex of plant Photosystem I (PSI) is characterized by extremely red-shifted and broadened absorption and emission bands from its low-energy chlorophylls (Chls). The mixing of a charge-transfer (CT) state with the excited state manifold causing these so-called red forms results in highly complicated multi-component excited energy transfer (EET) kinetics within the complex. The two-dimensional electronic spectroscopy experiments presented here reveal that EET towards the CT state occurs on three timescales: fast from the red Chls (within 1 ps), slower (5–7 ps) from the stromal side Chls, and very slow (100–200 ps) from a newly discovered 690 nm luminal trap. The excellent agreement between the experimental data with the previously presented Redfield–Förster exciton model of Lhca4 strongly supports the equilibration scheme of the bulk excitations with the dynamically localized CT on the stromal side. Thus, a complete picture of the energy transfer pathways leading to the population of the CT final trap within the whole Lhca4 complex is presented. In view of the environmental sensitivity of the CT contribution to the Lhca4 energy landscape, we speculate that one role of the CT states is to regulate the EET from the peripheral antenna to the PSI core.

Introduction

Photosystem I (PSI) is one of the key elements in the photosynthetic process by which plants, algae, and cyanobacteria convert solar energy into chemical energy. In plants, this multi-pigment–protein complex consists of a core complex (PSI core) and an outer antenna composed of light-harvesting complexes (LHCI). The PSI core, with about 98 protein-bound chlorophylls (Chls), contains the reaction center (RC) in which charge separation occurs. The LHCI enhance the PSI absorption cross-section, containing 57 Chls that transfer their excitation energy to the core.[1–4] The LHCI of plants is composed of four subunits (Lhca1–4), which are organized as heterodimers (Lhca2–3 and Lhca1–4) on one side of the core.[1,2] These subunits belong to the same large Lhc family which also includes the antenna complexes of Photosystem II (PSII), the Lhcbs.[5] All these complexes have a nearly identical structure

and very similar pigment organization.[1,2,5] However, characteristic for the Lhca subunits is the presence of several red spectral forms absorbing at an energy lower than that of the primary donor P_{700}. Interestingly, due to their position within the protein close to the core these red forms are part of the most probable energy transfer pathways of excitations from the light-harvesting subunits towards the core.[1,4–9] The forms originate from the so-called 'red Chls', which have a significantly red-shifted and broadened absorption and fluorescence emission spectra (absorbing at 708 nm and emitting at 733 nm) compared to the 'bulk Chl a' molecules in the antenna (absorbing up to 680 nm and emitting up to 686 nm[10]). Particularly in Lhca3 and Lhca4 prominent low-energy states are observed, with absorption and emission maxima respectively at 705 and 725 nm for Lhca3 and 708 nm and 733 nm for Lhca4.[11] By means of site-directed mutagenesis of the Lhca proteins the excitonically coupled Chl a dimer $a603$–$a609$ was identified to be the location of the red-shifted states.[10] Specifically, the Asparagine (Asn) residues coordinating Chl $a603$ within Lhca3 and Lhca4 are essential: mutation of this residue into Histidine (His), which is the natural ligand for Chl 603 in the other Lhc subunits, results in the loss of the red forms.[10,12,13] This mutant, Lhca4 N47H, has been used in several studies examining the properties of the red forms.[11,13,14]

Based on fluorescence data,[15] it was hypothesized that the red-shifted absorption and fluorescence originates from two different states. This was later confirmed by subsequent

[a] *Department of Biophysics, Faculty of Sciences, Vrije Universiteit Amsterdam and LaserLaB Amsterdam, De Boelelaan 1081, 1081 HV Amsterdam, The Netherlands. E-mail: m.tros@vu.nl*

[b] *A. N. Belozersky Institute of Physico-Chemical Biology, Moscow State University, Leninskie Gory, 119992 Moscow, Russia*

[c] *Institute of Chemical Research of Catalonia (ICIQ), Barcelona Institute of Science and Technology (BIST), Avinguda dels Països Catalans 16, 43007 Tarragona, Spain*

† Electronic supplementary information (ESI) available. See DOI: 10.1039/d0cp03351k

fluorescence line narrowing (FLN)[11] and Stark Spectroscopy experiments[16] on Lhca4. The two bands have a central wavelength of absorption at 690 and 708 nm and emission at 705 and 733 nm.[11] Furthermore, Stark spectroscopy showed that both these red forms originate from the mixing of the lowest Chl a exciton state delocalized over Chl $a603–a609$ with a charge-transfer (CT) state of that dimer.[16] The low energy exciton-CT mixed state couples strongly with phonons, resulting in a homogeneously broadened and extremely red-shifted emission band. As a result, the Huang–Rhys factor of the red Chls is more than three times larger than those of the other Chl a pigments within the antenna complex. The large coupling of the red forms to slow protein conformational motions results in the Lhcas having a very flexible energy landscape, showing reversible switching between conformations with and without red forms at room temperature (RT).[14] This indicates that the mixing of the CT state with the excitonic manifold is highly dynamic and strongly dependent on protein structural changes.

Due to the strong exciton-CT mixing in Lhca4, the quantitative description of its spectral properties is significantly more challenging than the modeling of pure excitonic spectra and dynamics. The high-resolution structure of the Lhca4 complex from Qin et al.[1] opened the possibility for the development of a quantitative theoretical exciton model which includes the CT state, which was done in a recent publication.[17] The model was based on monomeric reconstituted Lhca4, containing 12 Chls (9 Chl a and 3 Chl b) (Fig. 1). Using this model, a quantitative structure-based modeling of the cryogenic temperature (77 K) steady-state spectra (including absorption, linear dichroism, fluorescence, and Stark absorption) was performed. The fit of these spectra yields the model site energies, exciton couplings, disorder values and participation of the pigments in the adiabatic exciton states of all Lhca4 pigments including the CT state.[17] By including the strong exciton–phonon coupling of the mixed exciton-CT state, the resulting model was able to correctly describe all the spectral

characteristics of the red forms (and the other excitons). To obtain realistic dynamics it was shown that these Chls should be divided over 9 compartments (cmRgF-9 scheme) (differently colored in Fig. 1).[18] The energy transfer between the weakly interacting compartments was modeled by means of generalized Förster (gF) theory, whereas transfer between strongly mixed Chls within a compartment was described by coherent modified Redfield (cmR). Comparison of calculations with the Redfield–Förster cmRgF-9 and exact hierarchical equation of motion (HEOM) methods shows that the CT state, as well as all the states within the strongly coupled clusters containing the CT state, should be treated as dynamically localized,[18] that is, the mixing of the CT state with the low-energy Chl a states depends on reorganization dynamics of the phonon bath of the possible mixed states. Excitation near the crossing points of the potentials of the CT state and exciton/excited state can lead to an exciton-CT delocalized state. Subsequent reorganization towards the bottom of the CT potential results in the formation of a localized CT excited state.[18,19]

As it was shown in previous experimental studies,[3,9,20,21] the participation of the CT state in the excitonic landscape of Lhca4 also results in increased complexity of the excited energy transfer (EET) dynamics within the complex. It has been shown that equilibration of the energy harvested by Chls b and blue Chls a with the CT state is completed within a few ps.[20] However, the multi-exponential character of the kinetics within Lhca4 was not fully understood yet at that point. Especially a slow 500 ps component, found in previous time-resolved experiments,[3,13,20,22] could not be assigned to any specific energy transfer pathway.

To disentangle these different EET kinetics in Lhca4 and investigate the role of the CT state in light-harvesting new experimental evidence is needed. Two-dimensional electronic spectroscopy (2DES) has proven to be a particularly useful technique to study photosynthetic complexes involving almost dark states such as CT states.[23–30] 2DES[31,32] is able to directly
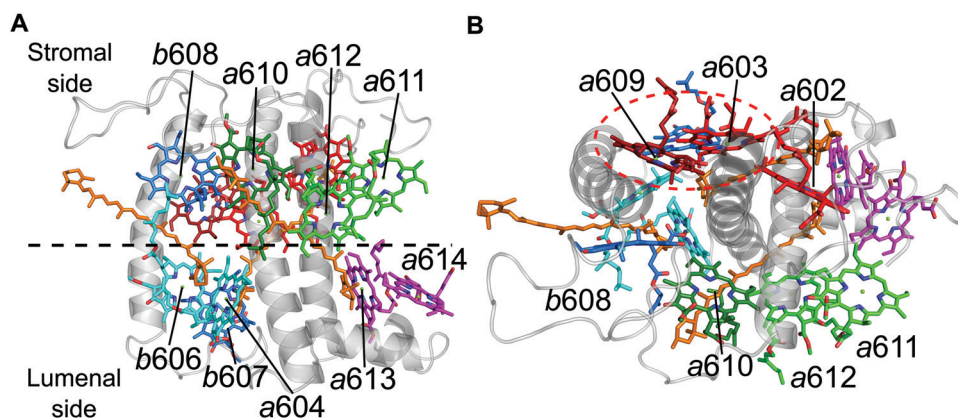
Fig. 1 Protein structure and pigment organization of monomeric reconstituted Lhca4. the structure and numbering of the Chls are from Qin et al.[1] (PDB ID: 4XK8). Pigment organization of Lhca4 viewed perpendicular to the membrane normal (A) and from the stromal side of the membrane (B). The different compartments of Chl clusters used in the cmRgF-9 model are indicated in different colors. The three carotenoids are all shown in orange. Chls 601, 617 and 618 are not shown as they are not present in reconstituted Lhca4.[17,18] The dashed black line indicates the division between stromal (top) and luminal (bottom) sides of the protein. The CT state is located on the red form Chls, $a603$ (red) and $a609$ (dark red), and are encircled with a dashed red line in panel B.

This journal is © the Owner Societies 2020

Phys. Chem. Chem. Phys., 2020, 22, 25720–25729 | 25721

correlate absorption to emission frequencies, as function of population time between excitation and emission events. The second dimension within the spectra gives an increased spectral resolution compared to conventional time-resolved absorption and fluorescence experiments, allowing for a better decomposition of overlapping transient spectral bands.[23] Therefore, 2DES experiments on Lhca4 will give more insight into the multi-exponential kinetics of the states underlying the red forms. Here, we combine experimental 2DES data on the Lhca4 wild-type (WT) and N47H mutant at both room temperature and 77 K with the recently reported Redfield theoretical model[18] to give a complete picture of the multiple energy transfer pathways leading to the population of the final trap (CT) within the whole Lhca4 complex for the first time.

Materials and methods

Mutagenesis and reconstitution

The N47H mutant has been obtained by the site-directed mutagenesis, in which the Chl 603-binding asparagine residue (N47) has been substituted by a Histidine (H).[3,10] Lhca4 WT and mutant N47H apoproteins overexpressed in *E.coli* of the Rosetta2 (DH3) strain and purified as inclusion bodies.[3] Reconstitution of Lhca4 WT and mutant N47H complexes was done as described previously for light-harvesting complex II (LHCII)[33] using the inclusion bodies and pigments (carotenoids and chlorophylls) isolated from spinach leaves. The reconstituted complexes were subsequently purified by His-tag Ni-affinity chromatography and sucrose density ultracentrifugation.[33] Ultracentrifugation was done on a 0.1–1 M sucrose gradient with 0.03% *n*-dodecyl-α-D-maltoside (α-DM), 10 mM Hepes pH 7.8 at 41 000 rpm (Beckman Coulter, SW41 rotor) at 4 °C for 18 h.

Steady-state spectroscopy

Absorption spectra at RT were recorded on a Varian Cary 4000 UV-Visible spectrophotometer (Varian, Palo Alto, CA). For the 77 K absorption spectra a homebuilt device was used. Fluorescence spectra were recorded at 77 K and RT on a Fluorolog 3.22 spectrofluorimeter (HORIBA JobinYvon-Spex, Longumeau, France). The sample was diluted to an optical density (OD) of <0.05 cm^{-1} at the Q_y maximum at 680 nm. For 77 K measurements a liquid nitrogen cooled device was used (cold finger).

2D electronic spectroscopy

2D electronic spectroscopy experiments were performed on a home-built diffractive optic-based inherently phase-stabilized four-wave mixing setup,[24,25] which is designed as previously reported.[34] The emitted photon-echo signal, resulting from the third-order optical response of the complexes by the interaction with a sequence of three subsequent ultrashort laser pulses,[31] is heterodyned with the low-intensity fourth local oscillator (LO) pulse and detected by a charge coupled device (CCD) camera (Princeton Instruments). The laser system (PHAROS, Light Conversion) was operating at a 1 KHz repetition rate. The laser pulses were generated by a home-built non-collinear

parametric amplifier (NOPA) and tuned to a central wavelength at 715 nm with a full width at half maximum (FWHM) of 80 nm (Fig. S1A, ESI†). The temporal width of the pulses was determined with frequency-resolved optical gating (FROG) of the second harmonic (SH) signal of beams 1 and 2 generated by a barium borate (BBO) crystal. From the autocorrelation signal (Fig. S1C, ESI†) of the resulting FROG profile (Fig. S1B, ESI†) the FWHM of the used 2DES pulses was calculated to be 15 fs. The pulse energy was set at 7 nJ per pulse and the spot diameter in the focus on the sample was ∼100 μm. A broad band pump–probe power study ensured no annihilation effects with the pulse energy employed. The sample was measured in a quartz cuvette with a path length of 500 μm with an optical density (OD) of 0.25 cm^{-1} in the Q_y absorption maximum. An oxygen scavenging mixture consisting of glucose oxidase 0.1 mg mL^{-1}, catalase 0.05 mg mL^{-1}, and glucose 10 mM was added to prevent sample degradation. The 77 K measurements were performed in a liquid nitrogen cooled cryostat (Optistat DN2, Oxford Instruments Nanoscience). To form an optical glass the 77 K sample solution consisted of 67% (w/v) glycerol.[13] The solution was buffered with 10 mM Hepes pH 7.8 and contained 0.03% α-DM. For the 77 K 2DES experiments, the coherence time τ was scanned from −130 to 275 fs with 1 fs step for the population times between −24 and 1200 fs with steps of 8 fs. For the RT measurements coherence times from −80 to 100 fs with 1 fs step were scanned for population times between −64 and 1600 fs with steps of 8 fs. Additional sets of spectra at longer population times were recorded at the following population times: T_{start}–step–T_{end} = 1.3–0.1–2.0 ps (1.8, 2.0 ps for RT), 3.0–1.0–10 ps, 20–10–100 ps, 250 and 500 ps.

Processing and analysis of the 2D spectra was done using a homebuilt python-based script. The 2D spectra were obtained by a protocol similar to the data-acquisition described previously.[34] The phase of the spectra was retrieved by means of the projection slice theorem (Fig. S2–S5, ESI†).[34–36] The datasets were globally[37] analyzed with a sequential model, in which the data is fit with a set of exponential decays that describe the evolution of the entire 2D spectrum. In this model the first component decays with the first lifetime into the next component, the second component with the second lifetime, and so on. For a complete fit of the entire 2D datasets three components were necessary for both WT and the N47H mutant, yielding three two-dimensional evolution associated decay spectra (EADS) with their corresponding lifetimes (which were all fitted in the analysis).

Results

The 2DES spectra of the Lhca4 WT and N47H mutant samples were measured at room (RT, 298 K) and cryogenic temperature (77 K). The experimental data measured at RT represents better the physiological working conditions of the complex. However, the enhanced resolution of the 77 K spectra allows for a better interpretation of the 2D data and identification of the underlying physical differences between the two samples investigated.
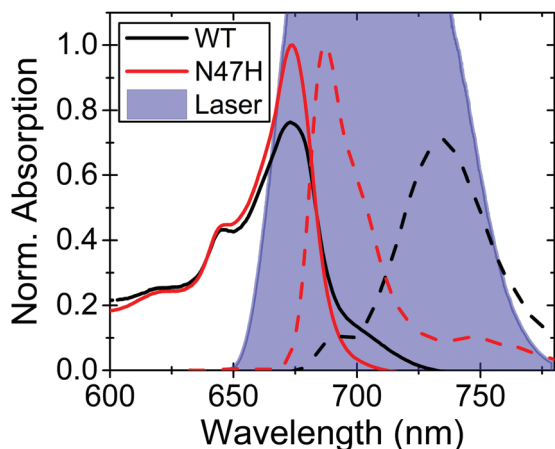
25722 | *Phys. Chem. Chem. Phys.*, 2020, **22**, 25720–25729

This journal is © the Owner Societies 2020

Fig. 2 Steady-state absorption and fluorescence spectra of Lhca4 WT and N47H mutant at cryogenic temperature (77K). 77 K absorption (solid) and emission (dashed) spectra of Lhca4 WT (black) and mutant N47H (red). Emission spectra were recorded after excitation with 475 nm light. Absorption spectra are normalized to the area within the 600–780 nm region. The emission spectra are normalized to the absorption, and then scaled to one at the N47H fluorescence maximum to facilitate the visualization of the spectra. Spectrum of the laser pulses utilized in the 2DES experiments is shown in blue, and scaled with FWHM at 1 to indicate that the laser spectrum covers the red side of the major Chl a Q$_y$ absorption band and the red forms region. The full laser spectrum is shown in Fig. S1 (ESI†).

Fig. 2 shows the 77 K absorption (solid) and 77 K emission (dashed) spectra of the Lhca4 WT and N47H mutant samples together with the spectral profile of the broadband laser pulses used in the 2DES experiments. The large Stokes shift ($\sim$55 nm or 1160 cm^{-1}, from absorption – maximum at 673 nm to fluorescence – maximum at 730 nm, Fig. 2) and the large broadening of the main emission band in WT are signatures of the mixed exciton-CT red form state.[38–40] At 77 K the emission of Lhca4 WT, dominated by the broad band centered at 730 nm, originates mainly from the red forms. In contrast, at RT (Fig. S6, ESI†) a smaller Stokes shift and a larger emission shoulder at 686 nm are observed, which can be ascribed to energy equilibration between other Chl states and the red forms. The absence of the red absorption shoulder ($>$700 nm) and of the broad red-shifted emission band ($\sim$730 nm) in the N47H mutant indicates the loss of the red form. Only an emission shoulder at $\sim$700 nm remains, which was seen in previous studies[10,11] and assigned to some weakly interacting CT states present in a small fraction of N47H mutant complexes.[17]

The laser pulses employed in the 2DES experiments (Fig. 2 and Fig. S6, ESI†) were optimized to probe both the low energy Chl a Q$_y$ states ($\sim$680 nm) as well as the broad red form band ($\sim$730 nm). The Chl b pigments ($\sim$650 nm) were not excited in these experiments. Fig. 3 shows the 77 K real rephasing 2D spectra at three different population times T. The elongated diagonal feature centered at [λ_τ,λ_t] = [680,682] nm in the early population times (T = 200 fs) for both WT and mutant corresponds to the ground state bleach (GSB) and stimulated emission (SE) prior to reorganization/energy transfer dynamics of the initially excited exciton states. The significant broader

signals along the diagonal for the WT sample as compared to the mutant at all T times are due to a fraction of the red forms being directly excited. The larger broadening in the anti-diagonal direction is also clearly observed in all the 2D spectra of the WT. Coupling of the exciton and exciton-CT mixed state to vibrations results in a complicated manifold of many excitonic and vibronic states contributing to these 2D spectra.[41] Moreover, the enhanced coupling of the CT state to slow and fast nuclear motions (slow conformational changes and fast vibrations) causes a high degree of inhomogeneous (disorder-induced) and homogeneous[39,42] (phonon-induced) broadening of the red form states,[17] respectively. The T = 5 ps spectrum of the WT sample shows an evident rise in the below-diagonal signal, indicating population of the red forms by EET from the lower energy Chl a excitonic state(s) in a few ps. In the N47H mutant spectrum, a similar below-diagonal rise is not observed, in agreement with the absence of the CT state. Instead, the excitation energy remains in the initially excited Chl a exciton state. In the WT, in the T = 50 ps spectrum the disappearance of the diagonal signal at [λ_τ,λ_t] = [680,682] nm and the appearance of a distinct cross peak at [λ_τ,λ_t] = [677,690] nm with a red tail extending up to 750 nm indicates the complete depopulation of the initially excited Chl a exciton states and the subsequent population of the terminal lowest energy red form state (Fig. 3B, red and 3C, grey). Furthermore, the presence of another diagonal peak centered at 690 nm, which becomes clear as the 680 nm signal decays, with a tail extending both on the diagonal and below diagonal indicates the presence of another long-lived red trap (the 690 nm trap). Energy transfer from this additional trap towards the exciton-CT state, causing the signal below the [688,690] nm diagonal band, occurs on a slow tens of ps timescale. In the N47H mutant, the lack of CT states produces a dominant 680 diagonal peak with only a small shoulder at [λ_τ,λ_t] = [672,685] nm below-diagonal. The absence of EET to CT determines the relatively high amplitude of the above diagonal negative excited state absorption (ESA) signal in the 50 ps 2D spectrum.[43] The long-lived diagonal signal at 690 nm is present also in the mutant (see the trace at [688,690] nm in Fig. 3B), however it is not discernible from the main diagonal [680,682] nm band in the 2D spectra. Fig. 3B reveals that the long-lived diagonal signal at [688,690] nm (normalized to the [680,682] nm main signal at T = 200 fs) are similar for the WT and N47H mutant. Due to a higher degree of spectral broadening at RT, the spectral changes in the 2D spectra at different times T (Fig. S7, ESI†) are less pronounced than in the 77 K spectra. However, similar features can be observed, the most important being the EET towards the red forms on a picosecond timescale.

In order to get a more thorough understanding of the dynamics and spectral evolution within the complexes, the transient kinetics at all points [λ_τ,λ_t] was simultaneously fit to a sum of exponentials in a global analysis[37] using a sequential model. With this analysis, the different decaying spectral species and their lifetimes can be separated. For WT the entire 2D kinetics could be fitted by a sum of three global exponentials, with respective lifetimes of 550 fs and 6.5 ps, and
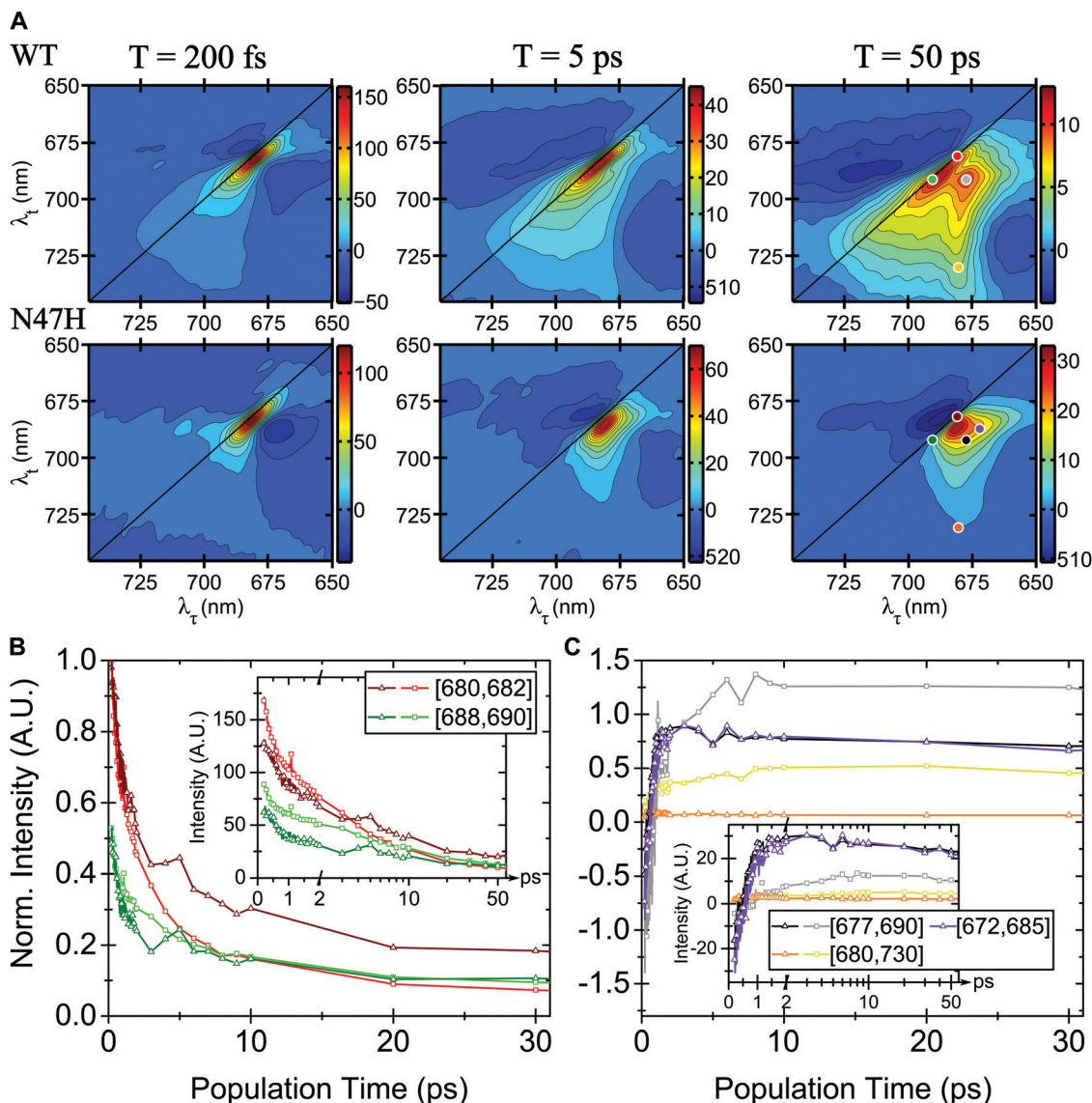
This journal is © the Owner Societies 2020

Phys. Chem. Chem. Phys., 2020, **22**, 25720–25729 | **25723**

Fig. 3 Real rephasing 2D spectra of Lhca4 at cryogenic temperature (77 K) and selected traces. (A) 77 K 2D spectra of WT (top) and N47H mutant (middle) Lhca4 at population times T = 200 fs, 5 ps and 50 ps. Transient kinetics of several diagonal (B) and anti-diagonal points (C) of the 77 K 2D spectra of WT (squares) and N47H mutant (triangles). The position of the chosen points is indicated in the zoomed-in 50 ps 2D spectra. The diagonal traces are normalized to the diagonal peak signal at (B) T = 200 fs and 50 ps (C). The insets of (B) and (C) show the original traces, with a linear scale for early population times T = 0–2 ps and a logarithmic scale for the range T = 2–50 ps.

a long-lived component that did not decay within the measured range of T (1 ns). The high resemblance between the fitted curves and the measured traces as shown in several representative points $[\lambda_\tau, \lambda_t]$ indicates that the dynamics within the 2D data are well captured by the global analysis procedure (Fig. S8, ESI†). The addition of a fourth component resulted in two identical components with the same lifetime and evolution associated decay spectra (EADS), indicating that no more than three spectral components can be distinguished by global analysis.

The 2D EADS with their respective decay lifetime are displayed in Fig. 4. For the WT, the first fast component with a lifetime of 550 fs is assigned to equilibration among the excited Chl a exciton states. The EADS of the slower 6.5 ps component

also shows a decay of Chl a excited states. The spectral signature corresponding to the EET from the lower energy Chl a excitonic state(s) to the exciton-CT state appears as an elongated cross-peak below diagonal ($[\lambda_\tau, \lambda_t]$ = [675,685–740 nm]). This signature starts to develop in EADS2, observed as a significant broadening in the signal towards this wavelength range, and is completed in EADS3. As was already seen in Fig. 3, the long-lived component also features the signal of the 690 nm trap at $[\lambda_\tau, \lambda_t]$ = [688,690] nm. The amount of excitation energy that is transferred to the CT state can be estimated by comparing the amplitudes of several spectral regions in EADS1 and EADS3. For this calculation, the total amplitude of the diagonal band (taken as the area comprised within 3.5 nm above and 9 nm below the diagonal line) in EADS1, which corresponds to the initial excitations, is compared with

25724 | *Phys. Chem. Chem. Phys.*, 2020, **22**, 25720–25729

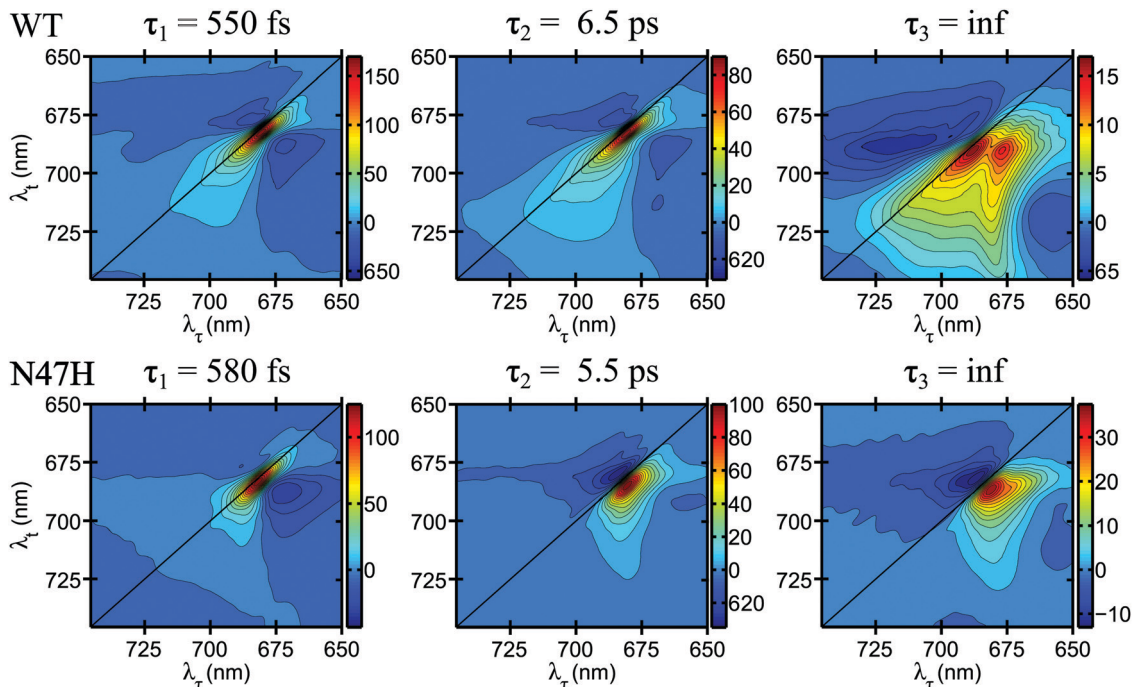This journal is © the Owner Societies 2020

Fig. 4 Global analysis of the 2D spectral evolution. Two-dimensional evolution associated decay spectra (EADS) of Lhca4 WT (top) and N47H (bottom) obtained in the global analysis of the entire 2D dataset (real rephasing). Respective decay time constants are indicated above each spectrum, the last decay time could not be accurately determined.

the diagonal area and the below-diagonal features (total area of all points in the 2D spectrum where $\lambda_t > \lambda_\tau - 3.5$ nm) of EADS3, which corresponds to the excitations on 690 red trap and the red form states, respectively. Hereby, it is estimated that $\sim$75% of the initial excitation energy reaches the final CT state. Notably, in this calculation it is assumed that all excitations from the long-lived 690 red trap (diagonal band in EADS3) are also transferred to the CT state. The $\sim$25% loss of excitations corresponds to the $\sim$25% quenching of energy from the high-energy (blue) Chl a excitons that was previously reported.[20]

For the N47H mutant similar decay lifetimes are obtained in the global analysis. Also here the evolution of the 2D spectra are properly described by the three components (Fig. S8, ESI†). As was seen in the 50 ps 2D spectrum (Fig. 3) a small shoulder from the diagonal was observed. However, this signal is located closer to the diagonal ($[\lambda_\tau,\lambda_t] = [672,685]$ nm) and significantly narrower than the cross-peak signal in the WT sample.

To investigate whether the developed Redfield–Förster cmRgF-9 compartmentalization scheme for the Lhca4 theoretical model and the resulting calculated energy transfer dynamics[18] are consistent, in the following we compare the measured 2DES kinetics as well as the kinetics from the global analysis to the dynamics calculated with the theoretical model. A more detailed description on the theoretical model and chosen parameters is given in the ESI† (Supplemental Methods).

In Fig. 5 the measured and calculated kinetics at the cross-peak [680, 730] nm (also shown in Fig. 3C, yellow) are compared. This point corresponds to the transfer from bulk Chls a (peaking near 680 nm) to the red form (giving the maximum of the steady-state emission near 730 nm[17]) and is therefore the

most relevant point to investigate the dynamics of EET from bulk Chls a to the CT state. The calculated kinetics (purple) overlap very well with the 2D data (black). The excellent agreement between experimental and modelled kinetics shown in Fig. 5, brings us to conclude that our current model is able to capture the details of the EET in Lhca4 including the presence and population dynamics of mixed-CT states with exceptional fidelity.
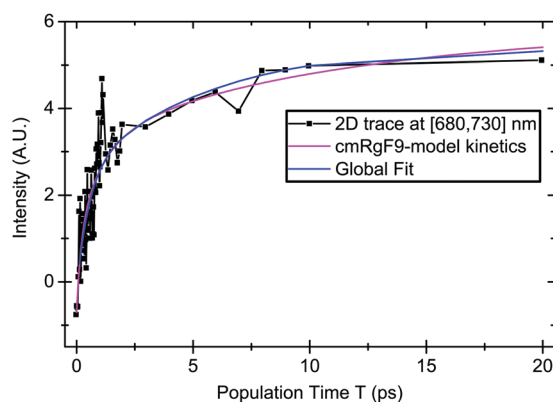

Fig. 5 2DES kinetics (real rephasing) at [680,730] nm for Lhca4 WT at cryogenic temperature (77 K). Measured data is shown by black points and the global analysis of the full 2D spectra is shown in the blue line. Calculated kinetics (magenta line) obtained by the cmRgF-9 Redfield–Förster model with averaging over disorder. In the model Chl clusters a602–603, a610, a611–612 and a613–614 were initially excited. All the parameters (site energies, exciton couplings, electron-phonon spectral density, disorder value, etc.) are the same as in our current model of Lhca4.[17]

This journal is © the Owner Societies 2020

Phys. Chem. Chem. Phys., 2020, **22**, 25720–25729 | **25725**

To understand in more detail the dynamics of the CT population and the origin of the 690 nm trap, it is useful to compare the kinetics calculated upon different initial conditions, *i.e.* the kinetics considering selective excitation of the different Chl pools within the model shown in Fig. 6. In Fig. 7 we show kinetics of EET to the red forms corresponding to excitation of some selected pigments (see Chl pools in Fig. 6) contributing to the 680 nm band (and therefore contributing to the [680, 730] nm cross-peak). The traces were normalized to the steady-state CT population. Supposing a selective excitation of the *a*603 site (red in Fig. 6) we obtain a fast (sub-ps) population of the CT (grey curve in Fig. 7). In this case, all excited state energy is transferred to the CT state within 1 ps. Excitation of the *a*602–603 (red in Fig. 6) sites results in slower kinetics due to the *a*602 → *a*603 relaxation (red curve). Notice that this is not a pure exciton-type relaxation, because in the presence of CT the *a*602 and 603 excited states are dynamically localized,[18] giving relatively slow equilibration within 3–4 ps (compare red and grey curves, Fig. 7). The kinetics are even slower if we also include *a*610–611–612 pigments (green curve). Note that in the cmRgF-9 model the *a*610 (dark green in Fig. 6) and *a*611–612 (green in Fig. 6) are considered as two separate clusters.[18] The equilibration between the localized *a*610 and other pigments is very slow in this model (about 20 ps, compare green and red/grey curves). In the global analysis these ps energy transfer processes are combined in the 6.5 ps component (Fig. 4), describing the EET from all stromal side Chls *a* towards the red forms. Including the luminal-side *a*613–614 pigments

(magenta in Fig. 6) further slows down the kinetics (see the differences between the magenta and green curves persisting even at very large delays, *i.e.* much more than 20 ps). Consequently, the 690 nm trap (Fig. 3 and 7) can be assigned to *a*613, and it is responsible for the previously unassigned and very slow (100–200 ps at 77 K) lumenal-to-stromal side transfers in Lhca4. Therefore, here we show that this pathway should be included to obtain the exceptional agreement between experiment and model shown in Fig. 5 and 7, and to achieve a complete physical picture of the energy transfer pathways within Lhca4.

Discussion

The 2D experiments presented here are the first experimental evidence explicitly showing the origins of the complex multi-component kinetics of the red form containing Lhca4 plant light-harvesting complex. We observe that EET from excited Chl *a* states to the red forms occurs on three different timescales: fast (within 1 ps) from the exciton states of the red Chls (*a*603 and *a*602 sites, dynamically coupled to the CT state located on *a*603–*a*609), slower (a few ps) transfers (determined by equilibration between the *a*602–603–CT cluster and other stromal side Chls *a*609, *a*610, *a*611–612) and very slow (100–200 ps) transfers to CT limited by equilibration between the stromal-side and lumenal-side Chls *a* (*i.e.* *a*604, *a*613–614). Superposition of these pathways determines a complicated multi-component kinetics of population of the final CT trap state. Since these CT chlorophylls are located close to the core,[1,5] the localization of excitations in the CT state could provide a directed energy transfer pathway from the peripheral LHCI antenna to the RC located in the PSI core.

The 2DES experiments shown here enable us to disentangle the spectral signatures of all these kinetic components and to present an accurate and complete picture of the energy transfer pathways within the Lhca4 antenna complex. Global analysis of the spectral evolution of the 2D spectra gives an accurate estimate of the timescales of the different processes underlying these separated signals. The second dimension λ_τ of the technique results in the separation of the spectral bands (see Fig. 7C) of the newly found 690 nm luminal red trap and the red form localized CT state. The results show that the 690 nm luminal red trap (located on Chl *a*613) is responsible for the very slow luminal-to-stromal energy transfer, which could not be assigned previously.[20]

For the N47H mutant, the below-diagonal signal observed in the Lhca4 WT has almost completely disappeared, and only a small off-diagonal signal remained. The source for this signal is probably the same as the 700 nm emission shoulder observed at 77 K (Fig. 2) and in previously reported emission spectra[10,11] and Stark absorption[16] data. Like previously hypothesized, this signal could be the result of a small fraction of N47H mutant complexes that still contain some weakly interacting CT states.[17] Although the 690 nm red trap should also be present in the mutant, no band can be distinguished at this wavelength
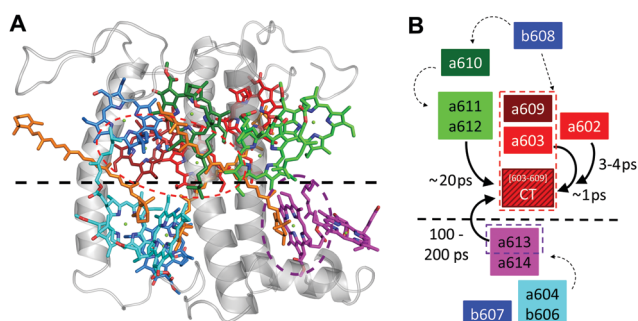

Fig. 6 Energy transfer pathways in Lhca4 leading to the population of the CT state. The structure and numbering of the Chls are from Qin *et al.*[1] (PDB ID: 4XK8). (A) Pigment organization of reconstituted Lhca4 viewed perpendicular to the membrane normal like in Fig. 1b. The different compartments of Chl clusters used in the cmRgF-9 model are indicated in different colors: Chl *a*602–603 (red), *a*609 (dark red), *a*611–612 (green), *a*610 (dark green) and *b*608 (blue) for the stromal side and *a*604–*b*606 (cyan), *a*613–614 (magenta) and *b*607 (blue) for the luminal side.[18] The three carotenoids are all shown in orange. The dashed black line indicates the division between stromal (top) and luminal (bottom) sides of the protein. The red form Chls (location of CT state), *a*603 (red) and *a*609 (dark red), and 690 nm luminal trap Chl *a*613 (purple), are encircled with respectively dashed red and purple lines. (B) For the interactions between the Chls within the complex a compartmentalization scheme was developed. energy transfer between Chls within the same cluster is described with cmR, while transfer between clusters (arrows) follows gF theory. Solid lines indicate energy transfer components assessed in this study, dashed lines are transfers previously discussed.[18]
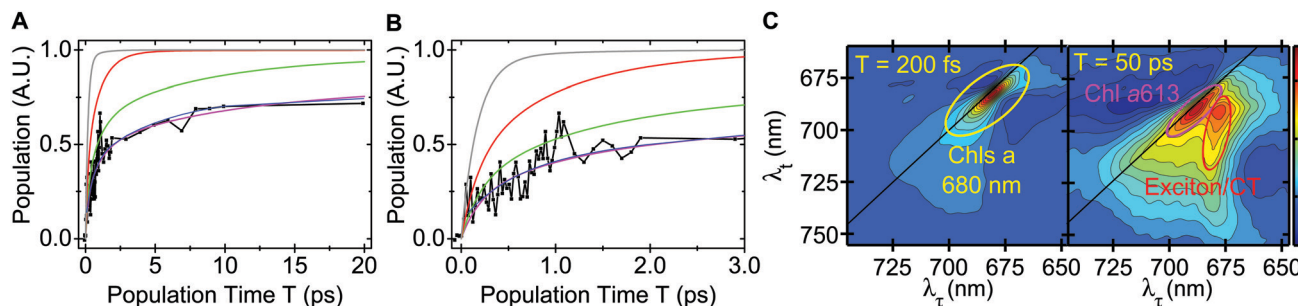
25726 | *Phys. Chem. Chem. Phys.*, 2020, **22**, 25720–25729

This journal is © the Owner Societies 2020

Fig. 7 Population of CT state of WT Lhca4. Kinetics of the CT population on the 20 ps (A) and 3 ps (B) timescales calculated for different initial conditions compared with the measured (680, 730) nm cross-peak (black line) and the dynamics of the cross-peak determined by the global analysis (blue line). The kinetics with realistic initial conditions (magenta) is compared with the kinetics corresponding to excitation of only $a603$ (grey), $a602-603$ (red), and $a602-603-610-611-612$ (green). The intensity of the kinetic traces has been normalized to the total excited state population after excitation. Measured 2D spectra at 200 fs and 50 ps delays (C) with major peaks assigned to respective pigments (see Fig. 1 and 6).

in the 50 ps spectrum and EADS3. However, at the point [688,690] nm, where the band is observed in WT, there is a significant positive signal (Fig. 3B). Moreover, the ESA negative signal above diagonal is more intense, which probably partly distorts the shape of the signal. Hereby, we consider that the 690 nm band is present in the mutant but is not discernible from the main 680 nm diagonal peak.

The experimental results were compared to the quantitative exciton model for Lhca4 WT which included mixing of the exciton states with the CT state.[17] For this model (based on the recently reported detailed crystal structure of PSI[1]) a compartmentalization scheme (Fig. 6B) was developed based on Redfield–Förster theory which describes the population dynamics.[18] The 2DES experiments of this study show that there is an excellent agreement between the dynamics predicted by the model and the observed 2DES kinetics, meaning that the model correctly describes initial excitation, inter-cluster equilibration and equilibration between luminal and stromal layers. More importantly, the excellent agreement between the modelled and measured kinetics verify the proposal that the CT state and all states that are strongly coupled to the CT state should be treated as dynamically localized.

The dynamically localized states in Lhca4 underline the high flexibility of the Lhca proteins and the significant changes in the light-harvesting properties upon changes in protein conformation.[14] The spectral properties as well as the excitation energy transfer dynamics are controlled by the exciton-CT mixing. By protein conformational changes the complex can switch between states with different spectroscopic characteristics, in which a strong exciton-CT mixing results in a state with broadened absorption around 700 nm that is lost in states where this mixing is weak. As it was already mentioned before, these red forms are part of the most probable energy transfer pathways of excitations from the light-harvesting subunits towards the core. Therefore, the change in mixing alters the directed energy transfer from the antenna to the PSI core via the CT state, controlling the delivery of excitations from the periphery to the core and thereby preventing over-excitation of PSI. In principle, the degree of mixing is determined by the energy gap between the exciton and CT states (an increase of

the gap breaks the exciton mixing). However, even at large exciton-CT energy differences the mixing of these states can be increased due to the presence of resonant vibrations (when vibrational modes of the lower state overlap with the zero-phonon line (ZPL) origin of the higher state).[19,26,28,41] Obviously, such resonance is dependent on the disorder induced by conformational dynamics of the environment. A thorough investigation of the coherent oscillations in the 2D kinetics will provide better insights into these resonances and the coupling and coherence between the Chls and CT state within this complex. This will be presented in a future publication.

Conclusion

In this study we successfully revealed the origins of the multi-component kinetics of EET within the red form containing Lhca4 pigment–protein complex: (i) The EET from the excited pigments towards the red form CT state occurs on three different timescales, shown in Fig. 6. (ii) There is direct evidence for the 690 nm red trap on the luminal side of the complex. The excellent agreement between the kinetics observed in the 2D experiments and those modelled using our exciton model of Lhca4 provides a detailed scheme of the energy transfer of the bulk excitations to the dynamically localized CT on the stromal side. The 2DES results give a complete picture of the energy transfer pathways leading to the population of the final trap (CT) within the whole Lhca4 complex. The strong involvement of the CT state in the Lhca4 EET transfer dynamics points to its possible role in regulating the EET from the peripheral antenna to the PSI core.

Conflicts of interest

There are no conflicts to declare.

Acknowledgements

This journal is © the Owner Societies 2020

Phys. Chem. Chem. Phys., 2020, **22**, 25720–25729 | **25727**

References

1 X. Qin, M. Suga, T. Kuang and J. R. Shen, Structural basis for energy transfer pathways in the plant PSI-LHCI supercomplex, *Science*, 2015, **348**, 989–995.

2 Y. Mazor, A. Borovikova, N. Nelson, I. Caspy and N. Nelson, Structure of the plant Photosystem I supercomplex at 2.6 Å resolution, *eLife*, 2015, **4**, 1–9.

3 F. Passarini, E. Wientjes, H. van Amerongen and R. Croce, Photosystem I light-harvesting complex Lhca4 adopts multiple conformations: red forms and excited-state quenching are mutually exclusive, *Biochim. Biophys. Acta, Bioenerg.*, 2010, **1797**, 501–508.

4 E. Wientjes, I. H. M. van Stokkum, H. van Amerongen and R. Croce, The role of the individual Lhcas in Photosystem I excitation energy trapping, *Biophys. J.*, 2011, **101**, 745–754.

5 R. Croce, A close view of Photosystem I, *Science*, 2015, **348**, 970–971.

6 E. Engelmann, G. Zucchelli, A. P. Casazza, D. Brogioli, F. M. Garlaschi and R. C. Jennings, Influence of the Photosystem I–Light Harvesting Complex I antenna domains on fluorescence decay, *Biochemistry*, 2006, **45**, 6947–6955.

7 C. Slavov, M. Ballottari, T. Morosinotto, R. Bassi and A. R. Holzwarth, Trap-limited charge separation kinetics in higher plant Photosystem I complexes, *Biophys. J.*, 2008, **94**, 3601–3612.

8 P. Akhtar, C. Zhang, Z. Liu, H. S. Tan and P. H. Lambrev, Excitation transfer and trapping kinetics in plant Photosystem I probed by two-dimensional electronic spectroscopy, *Photosynth. Res.*, 2018, **135**, 239–250.

9 J. A. Ihalainen, I. H. M. van Stokkum, K. Gibasiewicz, M. Germano, R. van Grondelle and J. P. Dekker, Kinetics of excitation trapping in intact Photosystem I of Chlamydomonas reinhardtii and Arabidopsis thaliana, *Biochim. Biophys. Acta, Bioenerg.*, 2005, **1706**, 267–275.

10 T. Morosinotto, J. Breton, R. Bassi and R. Croce, The nature of a chlorophyll ligand in Lhca proteins determines the far red fluorescence emission typical of Photosystem I, *J. Biol. Chem.*, 2003, **278**, 49223–49229.

11 R. Croce, A. Chojnicka, T. Morosinotto, J. A. Ihalainen, F. van Mourik, J. P. Dekker, R. Bassi and R. van Grondelle, The low-energy forms of Photosystem I light-harvesting complexes: spectroscopic properties and pigment-pigment interaction characteristics, *Biophys. J.*, 2007, **93**, 2418–2428.

12 T. Morosinotto, M. Mozzo, R. Bassi and R. Croce, Pigment-pigment interactions in Lhca4 antenna complex of higher plants Photosystem I, *J. Biol. Chem.*, 2005, **280**, 20612–20619.

13 E. Wientjes, G. Roest and R. Croce, From red to blue to far-red in Lhca4: How does the protein modulate the spectral properties of the pigments?, *Biochim. Biophys. Acta, Bioenerg.*, 2012, **1817**, 711–717.

14 T. P. J. Krüger, E. Wientjes, R. Croce, R. van Grondelle, T. P. J. Kruger, E. Wientjes, R. Croce and R. van Grondelle, Conformational switching explains the intrinsic multifunctionality of plant light-harvesting complexes, *Proc. Natl. Acad. Sci. U. S. A.*, 2011, **108**, 13516–13521.

15 G. Zucchelli, T. Morosinotto, F. M. Garlaschi, R. Bassi and R. C. Jennings, The low energy emitting states of the Lhca4 subunit of higher plant Photosystem I, *FEBS Lett.*, 2005, **579**, 2071–2076.

16 E. Romero, M. Mozzo, I. H. M. van Stokkum, J. P. Dekker, R. van Grondelle and R. Croce, The origin of the low-energy form of Photosystem I light-harvesting complex Lhca4: mixing of the lowest exciton with a charge-transfer state, *Biophys. J.*, 2009, **96**, L35–L37.

17 V. I. Novoderezhkin, R. Croce, M. Wahadoszamen, I. Polukhina, E. Romero and R. Van Grondelle, Mixing of exciton and charge-transfer states in light-harvesting complex Lhca4, *Phys. Chem. Chem. Phys.*, 2016, **18**, 19368–19377.

18 V. I. Novoderezhkin, R. Croce and R. van Grondelle, Dynamics of the mixed exciton and charge-transfer states in light-harvesting complex Lhca4: Hierarchical equation approach, *Biochim. Biophys. Acta, Bioenerg.*, 2018, **1859**, 655–665.

19 V. I. Novoderezhkin and R. van Grondelle, Modeling of excitation dynamics in photosynthetic light-harvesting complexes: exact versus perturbative approaches, *J. Phys. B: At., Mol. Opt. Phys.*, 2017, **50**, 124003.

20 K. Gibasiewicz, R. Croce, T. Morosinotto, J. A. Ihalainen, I. H. M. van Stokkum, J. P. Dekker, R. Bassi and R. van Grondelle, Excitation energy transfer pathways in Lhca4, *Biophys. J.*, 2005, **88**, 1959–1969.

21 A. N. Melkozernov, S. Lin, V. H. R. Schmid, H. Paulsen, G. W. Schmidt and R. E. Blankenship, Ultrafast excitation dynamics of low energy pigments in reconstituted peripheral light-harvesting complexes of Photosystem I, *FEBS Lett.*, 2000, **471**, 89–92.

22 J. A. Ihalainen, R. Croce, T. Morosinotto, I. H. M. van Stokkum, R. Bassi, J. P. Dekker and R. van Grondelle, Excitation decay pathways of Lhca proteins: a time-resolved fluorescence study, *J. Phys. Chem. B*, 2005, **109**, 21150–21158.

23 E. E. Ostroumov, R. M. Mulvaney, R. J. Cogdell and G. D. Scholes, Broadband 2D electronic spectroscopy reveals a carotenoid dark state in purple bacteria, *Science*, 2013, **340**, 52–56.

24 M. Ferretti, R. Hendrikx, E. Romero, J. Southall, R. J. Cogdell, V. I. Novoderezhkin, G. D. Scholes and R. van Grondelle, Dark states in the light-harvesting complex 2 revealed by two-dimensional electronic spectroscopy, *Sci. Rep.*, 2016, **6**, 20834.

25 C. Ramanan, M. Ferretti, H. Van Roon, V. I. Novoderezhkin and R. Van Grondelle, Evidence for coherent mixing of excited and charge-transfer states in the major plant light-

25728 | *Phys. Chem. Chem. Phys.*, 2020, **22**, 25720–25729

This journal is © the Owner Societies 2020

harvesting antenna, LHCII, *Phys. Chem. Chem. Phys.*, 2017, **19**, 22877–22886.

26 E. Romero, R. Augulis, V. I. Novoderezhkin, M. Ferretti, J. Thieme, D. Zigmantas and R. Van Grondelle, Quantum coherence in photosynthesis for efficient solar-energy conversion, *Nat. Phys.*, 2014, **10**, 676–682.

27 F. Ma, E. Romero, M. R. Jones, V. I. Novoderezhkin and R. van Grondelle, Both electronic and vibrational coherences are involved in primary electron transfer in bacterial reaction center, *Nat. Commun.*, 2019, **10**, 933.

28 F. D. Fuller, J. Pan, A. Gelzinis, V. Butkus, S. S. Senlik, D. E. Wilcox, C. F. Yocum, L. Valkunas, D. Abramavicius and J. P. Ogilvie, Vibronic coherence in oxygenic photosynthesis, *Nat. Chem.*, 2014, **6**, 706–711.

29 M. L. Flanagan, P. D. Long, P. D. Dahlberg, B. S. Rolczynski, S. C. Massey and G. S. Engel, Mutations to R. sphaeroides reaction center perturb energy levels and vibronic coupling but not observed energy transfer rates, *J. Phys. Chem. A*, 2016, **120**, 1479–1487.

30 A. Niedringhaus, V. R. Policht, R. Sechrist, A. Konar, P. D. Laible, D. F. Bocian, D. Holten, C. Kirmaier and J. P. Ogilvie, Primary processes in the bacterial reaction center probed by two-dimensional electronic spectroscopy, *Proc. Natl. Acad. Sci. U. S. A.*, 2018, **115**, 3563–3568.

31 G. S. Schlau-Cohen, J. M. Dawlaty and G. R. Fleming, Ultrafast multidimensional spectroscopy: Principles and applications to photosynthetic systems, *IEEE J. Sel. Top. Quantum Electron.*, 2012, **18**, 283–295.

32 E. L. Read, H. Lee and G. R. Fleming, Photon echo studies of photosynthetic light harvesting, *Photosynth. Res.*, 2009, **101**, 233–243.

33 A. Natali, L. M. Roy and R. Croce, In Vitro Reconstitution of Light-harvesting Complexes of Plants and Green Algae, *J. Visualized Exp.*, 2014, 1–13.

34 T. Brixner, T. Mancal, I. V. Stiopkin and G. R. Fleming, Phase-stabilized two-dimensional electronic spectroscopy, *J. Chem. Phys.*, 2004, **121**, 4221–4236.

35 J. D. Hybl, A. Albrecht Ferro and D. M. Jonas, Two-dimensional Fourier transform electronic spectroscopy, *J. Chem. Phys.*, 2001, **115**, 6606–6622.

36 D. M. Jonas, Two-dimensional femtosecond spectroscopy, *Annu. Rev. Phys. Chem.*, 2003, **54**, 425–463.

37 I. H. M. M. van Stokkum, D. S. Larsen and R. van Grondelle, Global and target analysis of time-resolved spectra, *Biochim. Biophys. Acta, Bioenerg.*, 2004, **1657**, 82–104.

38 W. W. Parson and A. Warshel, Spectroscopic properties of photosynthetic reaction centers. 2. Application of the theory to Rhodopseudomonas viridis, *J. Am. Chem. Soc.*, 1987, **109**, 6152–6163.

39 T. Renger, Theory of optical spectra involving charge transfer states: dynamic localization predicts a temperature dependent optical band shift, *Phys. Rev. Lett.*, 2004, **93**, 1–4.

40 L. M. P. Beekman, R. N. Frese, G. J. S. Fowler, R. Picorel, R. J. Cogdell, I. H. M. van Stokkum, C. N. Hunter and R. van Grondelle, Characterization of the light-harvesting antennas of photosynthetic purple bacteria by Stark spectroscopy. 2. LH2 complexes: influence of the protein environment, *J. Phys. Chem. B*, 1997, **101**, 7293–7301.

41 V. I. Novoderezhkin, E. Romero and R. van Grondelle, How exciton-vibrational coherences control charge separation in the Photosystem II reaction center, *Phys. Chem. Chem. Phys.*, 2015, **17**, 30828–30841.

42 T. Mančal, L. Valkunas and G. R. Fleming, Theory of exciton-charge transfer state coupled systems, *Chem. Phys. Lett.*, 2006, **432**, 301–305.

43 I. Stiopkin, T. Brixner, M. Yang and G. R. Fleming, Heterogeneous exciton dynamics revealed by two-dimensional optical spectroscopy, *J. Phys. Chem. B*, 2006, **110**, 20032–20037.

This journal is © the Owner Societies 2020

Phys. Chem. Chem. Phys., 2020, **22**, 25720–25729 | **25729**